Keldysh Institute • Publication search

Keldysh Institute preprints • Preprint No. 144, 2018

ISSN 2071-2898 (Print)
ISSN 2071-2901 (Online)

Chikitkin A.V., Rogov B.V.

Family of symmetric bicompact schemes with spectral resolution property for hyperbolic equations

Recommended form of bibliographic references: Chikitkin A.V., Rogov B.V. Family of symmetric bicompact schemes with spectral resolution property for hyperbolic equations // Keldysh Institute Preprints. 2018. No. 144. 27 p. doi:**10.20948/prepr-2018-144-e**
URL: **http://library.keldysh.ru/preprint.asp?id=2018-144&lg=e**

KELDYSH INSTITUTE OF APPLIED MATHEMATICS

Russian Academy of Sciences

A.V.Chikitkin, B.V.Rogov

Family of symmetric bicompact schemes with spectral resolution property for hyperbolic equations

Moscow — 2018

Aleksandr Viktorovich Chikitkin, Boris Vadimovich Rogov

Family of symmetric bicompact schemes with spectral resolution property for hyperbolic equations

For the numerical solution of nonstationary quasilinear hyperbolic equations, a family of symmetric semidiscrete bicompact schemes based on collocation polynomials is constructed in the one- and multidimensional cases. A dispersion analysis of semidiscrete bicompact schemes of fourth to eighth orders of accuracy in space is performed. Numerical examples are presented that demonstrate the ability of the bicompact schemes to adequately simulate wave propagation, including short waves, on highly nonuniform grids at long times. The properties of solutions of bicompact schemes in the problem of transfer of a stepwise initial profile are also considered.

Key words: hyperbolic equations, bicompact schemes, dispersion errors, wave propagation

This research was supported by the Russian Foundation for Basic Research, project N 18-01-00857-a.

Contents

1. Introduction

The numerical simulation of acoustic, electromagnetic, and elastic wave propagation over long distances at long times requires schemes with low dissipation and dispersion. An example of schemes with such properties is provided by widely used symmetric compact schemes, which have a better spectral resolution than classical symmetric difference schemes of the same order of accuracy [1-3]. Recently, a family of semidiscrete symmetric compact schemes with a good spectral resolution has been proposed in [4] for the numerical solution of multiscale problems arising in computational aeroacoustics and direct numerical modeling of turbulence. In [4] the sixth- and eighth-order accurate schemes from this family were called optimal in terms of their accuracy-to-complexity ratio. However, these schemes can be used only on uniform or slightly nonuniform grids [1, 5], since their stencil consists of at least three integer nodes in each spatial direction.

For the numerical solution of the 1D quasilinear transport equation, a semidiscrete bicompact scheme of fourth-order accuracy in space was constructed in [6] by using the method of lines on a spatial stencil consisting of one half-integer and two integer nodes located within a single grid cell. This scheme contains two difference equations, so its effective difference order, which is defined as the difference between the total number of stencil nodes and the number of equations in the scheme, is equal to unity and coincides with the order of the differential transport equation with respect to spatial variable. A consequence of this coincidence of the orders is that the differential and difference problems have the same number of boundary conditions. Moreover, in the case of a sign-definite transport velocity, the semidiscrete scheme can be solved by marching computations in space [6]. The order of accuracy of the bicompact scheme are preserved in the transition from uniform to highly nonuniform grids. To integrate the equations of the semidiscrete scheme with respect to time, A- and L-stable multistage diagonally implicit Runge-Kutta (RK) methods were proposed, which are computationally more efficient than fully implicit RK methods [7]. In [8-10] the scheme from [6] was extended to systems of equations and to the multidimensional case. However, the fourth order of approximation in space may be insufficient for the numerical solution of multiscale problems, which require schemes with a higher spectral resolution. Therefore, for the numerical solution of hyperbolic equations, a family of symmetric semidiscrete bicompact schemes of arbitrary even order of accuracy in space is constructed in [11]. The spatial stencils of implicit bicompact schemes consist of two integer and several fractional nodes located within a single grid cell; moreover, the grid function values in a cell are related by a collocation polynomial.

In this work, a dispersion analysis of schemes of fourth to eighth orders of accuracy in space from the family of semidiscrete bicompact schemes [11] is presented. It is shown that the phase error of the sixth- and eighth-order accurate bicompact schemes does not exceed 0.2% and 0.03%, respectively, in the entire range of dimensionless wave numbers. A number of numerical examples are presented that demonstrate the ability of the bicompact schemes to adequately simulate wave

propagation on highly nonuniform grids at long times. The properties of solutions of the bicompact schemes in the problem of transfer of a stepwise initial profile are also considered.

2. Bicompact schemes as compact collocation-type ones

Using the scalar quasilinear transport equation

$$\frac{\partial u}{\partial t}+\frac{\partial f(u)}{\partial x}=0,\ \frac{df(u)}{du}>0 \tag{1}$$

as an example, we show (see [11]) that semidiscrete bicompact schemes, including the fourth-order accurate one from [6], can be constructed by applying collocation polynomials. For this purpose, we first consider the ordinary differential equation (ODE)

$$u_x=\psi(x,u), \tag{2}$$

where the subscript x denotes differentiation with respect to x. On the x axis, we introduce a nonuniform grid of integer nodes x_j with steps $h_{x,j+1/2}=x_{j+1}-x_j$. Since the subsequent presentation is concerned with only one spatial cell $[x_j,x_{j+1}]$, the second index on $h_{x,j+1/2}$ is omitted. Assume that we are given *nodal coefficients* (hereafter, for brevity, *nodes*) of collocation, i.e., real numbers $c_\alpha\in[0,1]$, $\alpha=\overline{1,s}$, where $s\ge 3$ is a positive integer. The collocation nodes are assumed to be symmetric with respect to the midpoints of the interval $[0,1]$ and $c_1=0$, $c_s=1$. An approximate solution of Eq. (2) with initial condition $u(x_j)=u_j$ on the interval $[x_j,x_j+h_x]$ is sought in the form of a collocation polynomial $p_s(x)$ of degree s satisfying the conditions

$$p_s'(x_j+c_\alpha h_x)=\psi(x_j+c_\alpha h_x,p_s(x_j+c_\alpha h_x)),\ \alpha=\overline{1,s},\ p_s(x_j)=u_j\ ,$$

where $p_s'(x)=dp_s/dx$. We introduce the following notation:

$$u_{j_\alpha}=p_s(x_{j_\alpha}),\ \psi_{j_\alpha}=\psi(x_{j_\alpha},u_{j_\alpha}),\ x_{j_\alpha}=x_j+c_\alpha h_x,\ \alpha=\overline{1,s} \tag{3}$$

where $j_\alpha\equiv j+c_\alpha$. The derivative of $p_s(x)$ can be uniquely expressed using a Lagrange interpolating polynomial:

$$p_s'(x_j+\xi h_x)=\sum_{\beta=1}^{s}\psi_{j_\beta}l_\beta(\xi),\ l_\beta(\xi)=\prod_{\substack{\alpha=1,\ldots,s\\ \alpha\ne\beta}}\frac{\xi-c_\alpha}{c_\beta-c_\alpha},\ \xi\in[0,1] \tag{4}$$

Integrating the left equality in (4) with respect to ξ on the intervals $[c_\alpha, c_{\alpha+1}]$ ($\alpha = \overline{1, s-1}$) and taking into account notation (3), we obtain $s-1$ linearly independent relations between u_{j_α} and ψ_{j_α}:

$$u_{j_{\alpha+1}} - u_{j_\alpha} = h_x \sum_{\beta=1}^{s} a_{\alpha\beta} \psi_{j_\beta}, \quad \alpha = \overline{1, s-1} \tag{5}$$

where

$$a_{\alpha\beta} = \int_{c_\alpha}^{c_{\alpha+1}} l_\beta(\xi) d\xi, \quad \alpha = \overline{1, s-1}, \ \beta = \overline{1, s} \tag{6}$$

System (5) is a one-step collocation difference scheme for integrating ODE (2) and is equivalent to an implicit RK method [7]. The stencil of this scheme consists of two integer nodes and $s-2$ fractional nodes. Equations (5) can also be treated as a system of equations for determining $s-1$ grid functions, namely, the basic function $\{u_j\}$ defined at integer nodes and the auxiliary functions $\{u_{j_\alpha}\}$ ($\alpha = \overline{2, s-1}$) defined at fractional nodes. The effective difference order of system (5), which is defined as the difference between the total number of stencil nodes and the total number of equations, is equal to unity. As a result, Eqs. (5) can be solved by the marching method with respect to *x*.

In what follows, we need the stability function [7] of the one-step scheme (5) for ODE (2) with a linear right-hand side $\psi(x,u) = \lambda u$, $\lambda = const$, i.e., for the linear Dahlquist equation [7]. In this case, scheme (5) becomes

$$u_{j_{\alpha+1}} - u_{j_\alpha} = z \sum_{\beta=1}^{s} a_{\alpha\beta} u_{j_\beta}, \quad z = \lambda h_x, \ \alpha = \overline{1, s-1}. \tag{7}$$

where λ is generally a complex constant. The stability function $R(z)$ of scheme (7) relates the grid function values at neighboring integer nodes:

$$u_{j+1} = R(z) u_j \tag{8}$$

where $u_{j+1} = u_{j_s}$, $u_j = u_{j_1}$, since $c_1 = 0$, $c_s = 1$.

For the ODE

$$f(u)_x = \psi(x,u) \tag{9}$$

a collocation difference scheme similar to scheme (5) for Eq. (2) has the form

$$f_{j_{\alpha+1}} - f_{j_\alpha} = h_x \sum_{\beta=1}^{s} a_{\alpha\beta} \psi_{j_\beta}, \quad f_{j_\alpha} = f(u_{j_\alpha}), \ \alpha = \overline{1, s-1} \tag{10}$$

To obtain a semidiscrete scheme (i.e., difference in x and continuous in t) for transport equation (1), we set $\psi = -\partial u/\partial t$ on the right-hand side of Eq. (9). Making the substitution $\psi = -\partial u/\partial t$ in (10) yields the system of evolution ODEs

$$h_x \sum_{\beta=1}^{s} a_{\alpha\beta} (\partial u/\partial t)_{j_\beta} + f_{j_{\alpha+1}} - f_{j_\alpha} = 0, \ \alpha = \overline{1, s-1} \tag{11}$$

which is a semidiscrete difference scheme for Eq. (1). Note that other equivalent forms of this scheme can be obtained by setting up independent linear combinations of Eqs. (11).

If s = 3 and the collocation nodes are evenly spaced ($c_1 = 0$, $c_2 = 1/2$, $c_3 = 1$), scheme (11) consists of two equations with the coefficient matrix $\mathbf{A} = \{a_{\alpha\beta}\}$ given by

$$\mathbf{A} = \mathbf{A}_4 = \begin{bmatrix} \frac{5}{24} & \frac{1}{3} & -\frac{1}{24} \\ -\frac{1}{24} & \frac{1}{3} & \frac{5}{24} \end{bmatrix} \tag{12}$$

Adding up these equations and subtracting them from one another, we obtain an equivalent scheme

$$\begin{aligned} &\frac{h_x}{6}\left[\left(\frac{\partial u}{\partial t}\right)_j + 4\left(\frac{\partial u}{\partial t}\right)_{j+1/2} + \left(\frac{\partial u}{\partial t}\right)_{j+1}\right] + f_{j+1} - f_j = 0, \\ &\frac{h_x}{4}\left[\left(\frac{\partial u}{\partial t}\right)_j - \left(\frac{\partial u}{\partial t}\right)_{j+1}\right] - (f_{j+1} - 2f_{j+1/2} + f_j) = 0. \end{aligned} \tag{13}$$

Scheme (13) coincides with the semidiscrete bicompact one from [6], which is fourth-order accurate in x [8-10]. The subscript on $\mathbf{A}$ in (12) shows the order of accuracy of the scheme in x. Note that the collocation nodes of this scheme are the nodes of the Lobatto quadrature formula [7], which are the roots of the polynomial

$$\frac{d^{s-2}}{dx^{s-2}}\left(x^{s-1}(x-1)^{s-1}\right)$$

The stability function of scheme (7) with the coefficient matrix $\mathbf{A}_4$ has the form

$$R(z) = R_4(z) \equiv \frac{z^2 + 6z + 12}{z^2 - 6z + 12} \tag{14}$$

and is the (2,2)-Padé approximant of the exponential e^z. Let $z = x + iy$, where x and y are real values and i is the imaginary unit. Then, from formula (14), we conclude that scheme (7) with the coefficient matrix (12) is (i) A-stable [7], i.e., $|R(z)| \le 1$ for $\mathrm{Re}\, z \le 0$; and (ii) monotone [12, p. 41], i.e., A-stable and $R(x) > 0$ for $x \le 0$.

If $s = 5$ and the collocation nodes are evenly spaced $(c_1 = 0,\ c_2 = 1/4,\ c_3 = 1/2,\ c_4 = 3/4,\ c_5 = 1)$, then scheme (11) consists of four equations with the coefficient matrix given by

$$\mathbf{A} = \mathbf{A}_6 = \frac{1}{2880}\begin{bmatrix} 251 & 646 & -264 & 106 & -19 \\ -19 & 346 & 456 & -74 & 11 \\ 11 & -74 & 456 & 346 & -19 \\ -19 & 106 & -264 & 646 & 251 \end{bmatrix} \tag{15}$$

The stability function of scheme (7) with the coefficient matrix $\mathbf{A}_6$ has the form

$$R(z) = R_6(z) \equiv \frac{3z^4 + 50z^3 + 420z^2 + 1920z + 3840}{3z^4 - 50z^3 + 420z^2 - 1920z + 3840} \tag{16}$$

and satisfies

$$|R(z)| \le 1 \ \text{при}\ \mathrm{Re}\, z \le 0;\ R(x) > 0 \ \text{при}\ x \le 0. \tag{17}$$

The fulfillment of conditions (17) means that scheme (7) with the coefficient matrix $\mathbf{A}_6$ is A-stable and monotone.

In the case of $s = 5$ and evenly spaced collocation nodes $(c_1 = 0,\ c_2 = 0.5 - \sqrt{3/28},\ c_3 = 0.5,\ c_4 = 0.5 + \sqrt{3/28},\ c_5 = 1)$, which are nodes of the Lobatto quadrature formula, scheme (11) also consists of four equations with the coefficient matrix given by

$$\mathbf{A} = \mathbf{A}_8 = \frac{1}{141120} \times \begin{bmatrix} 8568 + 216\sqrt{21} & 19208 - 504\sqrt{21} & 25088 - 6144\sqrt{21} & 19208 - 3864\sqrt{21} & -1512 + 216\sqrt{21} \\ -2835 - 216\sqrt{21} & 5649\sqrt{21} & 6144\sqrt{21} & -1281\sqrt{21} & 2835 - 216\sqrt{21} \\ 2835 - 216\sqrt{21} & -1281\sqrt{21} & 6144\sqrt{21} & 5649\sqrt{21} & -2835 - 216\sqrt{21} \\ -1512 + 216\sqrt{21} & 19208 - 3864\sqrt{21} & 25088 - 6144\sqrt{21} & 19208 - 504\sqrt{21} & 8568 + 216\sqrt{21} \end{bmatrix} \tag{18}$$

The stability function of scheme (7) with the coefficient matrix $\mathbf{A}_8$ has the form

$$R(z) = R_8(z) \equiv \frac{z^4 + 20z^3 + 180z^2 + 840z + 1680}{z^4 - 20z^3 + 180z^2 - 840z + 1680} \tag{19}$$

and is the (4,4)-Padé approximant of the exponential e^z. This function satisfies inequalities (17); therefore, scheme (7) with the coefficient matrix $\mathbf{A}_8$ is A-stable and monotone.

Based on collocation polynomials, the method for constructing schemes (11), (15) and (11), (18) implies that their order of accuracy in space is equal to six and eight, respectively [7]. In Section 4, this conclusion will be confirmed by numerical computations.

With the help of collocation polynomials, it is easy to construct bicompact schemes in several dimensions. For simplicity, we show this in the two-dimensional case. First, consider the stationary quasilinear transport equation

$$f(u)_x + g(u)_y = \psi(x, y, u) \tag{20}$$

The semidiscrete scheme (10) for Eq. (9) is rewritten as

$$\sum_{\beta=1}^{s} b_{\alpha\beta} f_{j_\beta} = h_x \sum_{\beta=1}^{s} a_{\alpha\beta} \psi_{j_\beta}, \quad \alpha = 1, \ldots, s-1 \tag{21}$$

where the elements of the matrix $\mathbf{B} = \{b_{\alpha\beta}\}$ are given by the formulas

$$b_{\alpha\beta} = \begin{cases} -1, \beta = \alpha \\ 1, \beta = \alpha + 1 \\ 0, \beta \neq \alpha, \alpha + 1 \end{cases}, \ \alpha = \overline{1, s-1}, \ \beta = \overline{1, s} \tag{22}$$

For the equation

$$g(u)_y = \psi(y, u) \tag{23}$$

we use a difference scheme similar to (21), namely,

$$\sum_{\beta=1}^{s} b_{\alpha\beta} g_{k_\beta} = h_y \sum_{\beta=1}^{s} a_{\alpha\beta} \psi_{k_\beta}, \quad \alpha = 1, \ldots, s-1, \tag{24}$$

where $k_\beta \equiv k + c_\beta$ and k is used to index the integer grid nodes on the y axis. For Eq. (20), applying the same x-discretization as in deriving scheme (21) for Eq. (9) and, then, the same y-discretization as in deriving scheme (24) for Eq. (23), we obtain a two-dimensional bicompact scheme with equations

$$h_y \sum_{\alpha=1}^{s} \sum_{\beta=1}^{s} a_{\alpha'\beta} b_{\beta'\alpha} f_{j_\alpha k_\beta} + h_x \sum_{\alpha=1}^{s} \sum_{\beta=1}^{s} a_{\beta'\alpha} b_{\alpha'\beta} g_{j_\alpha k_\beta} = h_x h_y \sum_{\alpha=1}^{s} \sum_{\beta=1}^{s} a_{\beta'\alpha} a_{\alpha'\beta} \psi_{j_\alpha k_\beta}, \quad \alpha', \beta' = \overline{1, s-1} \tag{25}$$

where $f_{j_\alpha k_\beta} = f(u_{j_\alpha k_\beta}), g_{j_\alpha k_\beta} = g(u_{j_\alpha k_\beta}), \psi_{j_\alpha k_\beta} = \psi(x_{j_\alpha}, y_{k_\beta}, u_{j_\alpha k_\beta}), y_{k_\beta} = y_k + c_\beta h_y$, and $u_{j_\alpha k_\beta}$ is the grid function value at the node $(x, y) = (x_{j_\alpha}, y_{k_\beta})$. To derive a bicompact scheme for the nonstationary homogeneous transport equation

$$u_t + f(u)_x + g(u)_y = 0 \tag{26}$$

we formally substitute $\psi(x, y, u) = -u_t$ into Eqs. (25) to obtain

$$h_x h_y \sum_{\alpha=1}^{s}\sum_{\beta=1}^{s} a_{\beta'\alpha} a_{\alpha'\beta} (u_t)_{j_\alpha k_\beta} + h_y \sum_{\alpha=1}^{s}\sum_{\beta=1}^{s} a_{\alpha'\beta} b_{\beta'\alpha} f_{j_\alpha k_\beta} + h_x \sum_{\alpha=1}^{s}\sum_{\beta=1}^{s} a_{\beta'\alpha} b_{\alpha'\beta} g_{j_\alpha k_\beta} = 0, \quad \alpha', \beta' = \overline{1, s-1} \tag{27}$$

If high-order accurate multistage diagonally implicit RK methods are used to integrate ODE system (27), the system of difference equations arising at every stage of these methods can be efficiently solved using iterated approximate factorization [13].

3. Dispersion properties of semidiscrete bicompact schemes

The dispersion properties of the fourth- and sixth-order accurate bicompact schemes (13) and (11), (15) were examined in [11,14]. In [15] an optimized semidiscrete symmetric bicompact scheme of the sixth-order accurate was found; it has a group velocity that deviates least from the exact group velocity. In this paper, the analysis of dispersion properties of the eight-order bicompact scheme (11), (18) is presented for the first time. However, to compare the properties of bicompact schemes with different orders of accuracy, we also present the results of the dispersion analysis for the fourth- and sixth-order schemes from [11,14].

The dispersion and dissipation of a scheme is usually estimated using the Cauchy problem for Eq. (1) with a linear function

$$f(u) = cu, \ c = const > 0 \tag{28}$$

periodic initial data $u(x, 0) = \exp(ikx)$, and the exact solution

$$u(x, t) = e^{ik(x-ct)} \tag{29}$$

where k is the physical (exact) wave number and c is the phase velocity.

According to formula (11), the bicompact scheme from Section 2 for Eq. (1) with function (28) has the form

$$h_x \sum_{\beta=1}^{s} a_{\alpha\beta} (\partial u/\partial t)_{j_\beta} + c(u_{j_{\alpha+1}} - u_{j_\alpha}) = 0, \ \alpha = \overline{1, s-1} \tag{30}$$

The basic semidiscrete function $u_m(t)$ in (30) (which is defined at integer nodes) is sought in the form of a traveling wave

$$u_m(t) = e^{ik(x_m - c^* t)} = e^{ikx_m} e^{-ik^* ct}, \ m = j, j+1, \tag{31}$$

where c^* is the numerical phase velocity, $k^* = kc^*/c$ is the effective (numerical) wave number [16], and $u_{j_\alpha}(t)$ are auxiliary semidiscrete functions defined at fractional nodes as

$$u_{j_\alpha}(t) = \rho_{\alpha-1} e^{ikx_{j_\alpha}} e^{-ik^* ct}, \ \rho_{\alpha-1} = const, \ \alpha = \overline{2, s-1}. \tag{32}$$

Substituting functions (31) and (32) into the system of linear ODES (30), we derive $s-1$ algebraic equations for determining $s-1$ unknowns: ρ_α ($\alpha = \overline{1, s-2}$) and the dimensionless effective wave number $\varphi^* = k^* h_x$. It follows from (31) and (32) that

$$(\partial u/\partial t)_{j_\beta} = -ik^* c u_{j_\beta}, \ \beta = \overline{1, s},$$

Therefore, Eq. (30) yields the following relation between these functions:

$$u_{j_{\alpha+1}} - u_{j_\alpha} = ik^* h_x \sum_{\beta=1}^{s} a_{\alpha\beta} u_{j_\beta}, \ \alpha = \overline{1, s-1}. \tag{33}$$

Comparing Eqs. (7) with (33) and taking into account (8), we obtain the following relation between functions (31) at integer nodes:

$$u_{j+1} = R(i\varphi^*) u_j \tag{34}$$

where $R(z)$ is the stability function of the one-step scheme (7). Substituting (31) into formula (34) yields the relation between φ^* and the dimensionless wave number $\varphi = kh_x$:

$$R(i\varphi^*) = e^{i\varphi}. \tag{35}$$

Note that formulas (14), (16), and (19) imply that

$$\left| R_m(i\varphi^*) \right| = 1, \ m = 4, 6, 8,$$

Therefore, a solution of Eq. (35) exists if $R(z)$ is the stability function $R_m(z)$, $m = 4, 6, 8$. Consider the solutions of Eq. (35) for these stability functions.

For the fourth-order accurate semidiscrete bicompact scheme (30) with the coefficient matrix $\mathbf{A}_4$, Eq. (35) with $R(z) = R_4(z)$ can be transformed into

$$(\varphi^*)^2 + 6\cot(\varphi/2)\varphi^* - 12 = 0. \qquad (36)$$

From (36), we obtain an explicit dependence of φ on φ^*:

$$\varphi = 2\arctan\left(\frac{6\varphi^*}{12-(\varphi^*)^2}\right). \qquad (37)$$

Dependence (37) for $\varphi \in [-\pi, \pi]$ is depicted by three curves in Fig. 1. These curves do not intersect; moreover, only one of them (curve *1*) passes through the point (0,0) in the (φ, φ^*) plane and corresponds to the physical solution.

Since function (37) is odd, the subsequent consideration is restricted to the case $\varphi \in [0, \pi]$. Dependence (37) is easy to invert on curve *1* to obtain

$$\varphi^* = 3\left[\sqrt{\cot^2(\varphi/2) + 4/3} - \cot(\varphi/2)\right], \ \varphi \in [0, \pi]. \qquad (38)$$

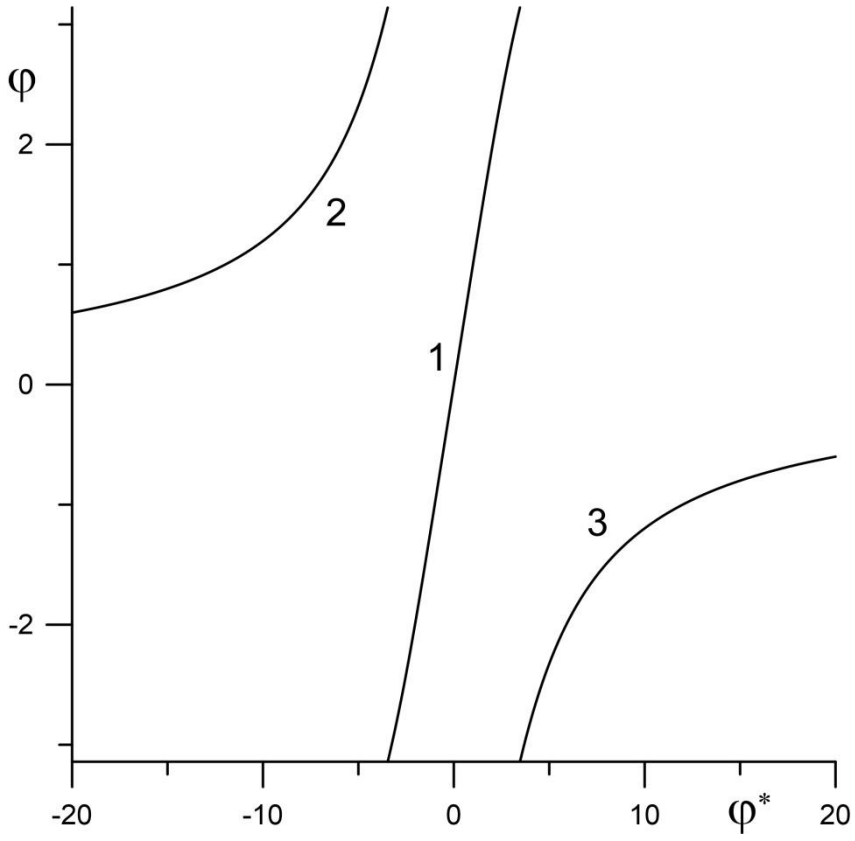

Fig. 1. The dimensionless exact wave number as a function of the dimensionless effective wave number for the semidiscrete bicompact scheme of the 4th order of accuracy.

For the fourth-order bicompact scheme, the group velocity c_g of a wave packet is given by

$$\frac{c_g}{c}=\frac{d\varphi^*}{d\varphi}=\frac{3}{2\sin^2(\varphi/2)}\left(1-\frac{1}{\sqrt{1+4\tan^2(\varphi/2)/3}}\right)$$

which is positive for all dimensionless wave numbers. Therefore, when applied to the computation of wave propagation on a highly nonuniform grid, this scheme does not lead [14] to wave reflection from the grid or the formation of spurious waves [17-19].

As was noted above, the effective difference order of the system of differential-difference equations (30) is equal to unity and coincides with the order of differential equation (1) in *x*. To use scheme (30), we need to specify only one boundary condition on the left, which coincides with the boundary condition for Eq. (1) with function (28) (i.e., no additional boundary condition on the right is required). Therefore, only one branch of the solution to Eq. (37) participates in the formation of the numerical solution. This branch is determined by a single boundary condition and is described by curve *1* in Fig. 1. If the effective difference order of scheme (30) were higher than unity and, accordingly, the number of difference boundary conditions were more than one, such a scheme would be capable of maintaining spurious numerical waves [3, p. 539].

Figure 2 displays the dimensionless effective wave number φ^* as a function of the dimensionless exact wave number φ for several symmetric compact schemes. The thick straight line depicts the ideal dependence $\varphi^*=\varphi$. In Fig. 3 the dimensionless numerical group velocity $c_g/c=d\varphi^*/d\varphi$ is plotted as a function of φ for the same schemes as in Fig. 2. Inspection of Fig. 3 shows that the dimensionless numerical group velocity is positive in the case of the fourth-order bicompact scheme and nonnegative in the case of the fourth-order compact scheme CCS-T4 [4] for all wavelengths. The traditional tridiagonal compact schemes of fourth, sixth, and eighth orders of accuracy from [20] yield negative group velocities in the short wavelength range. Note that, according to the group velocity control theory for shock-capturing schemes [21, 22], the bicompact scheme is of the fast type, while CCS-T4 [4] and traditional compact schemes are of the slow type.

The phase error of a scheme is usually characterized by the quantity $\left|\varphi^*/\varphi-1\right|=\left|c^*/c-1\right|$. Figure 2 shows that this error for CCS-T4 [4] is more than twice as large as that for the bicompact scheme. The maximum phase errors for the bicompact scheme and CCS-T4 [4] are 10.3% and 23.6%, respectively. They are observed at the shortest wavelength resolvable by the grid, which corresponds to $\varphi=\pi$. Note that the fourth-order bicompact scheme and CCS-T4 [4] both contain two difference equations. At the same time, the stencil of the former consists of two integer nodes and one half-integer node, while the stencil of the latter is composed of three integer and three half-integer nodes.

For the sixth-order accurate semidiscrete bicompact scheme (30) with the coefficient matrix $\mathbf{A}_6$, Eq. (35) with $R(z) = R_6(z)$ can be transformed into

$$3(\varphi^*)^4 + 50\cot(\varphi/2)(\varphi^*)^3 - 420(\varphi^*)^2 - 1920\cot(\varphi/2)\varphi^* + 3840 = 0. \qquad (39)$$

From Eq. (39), φ can be explicitly expressed in terms of φ^*:

$$\varphi = 2\arctan\left(\frac{\varphi^*\left[1920 - 50(\varphi^*)^2\right]}{3\left[(\varphi^*)^4 - 140(\varphi^*)^2 + 1280\right]}\right). \qquad (40)$$

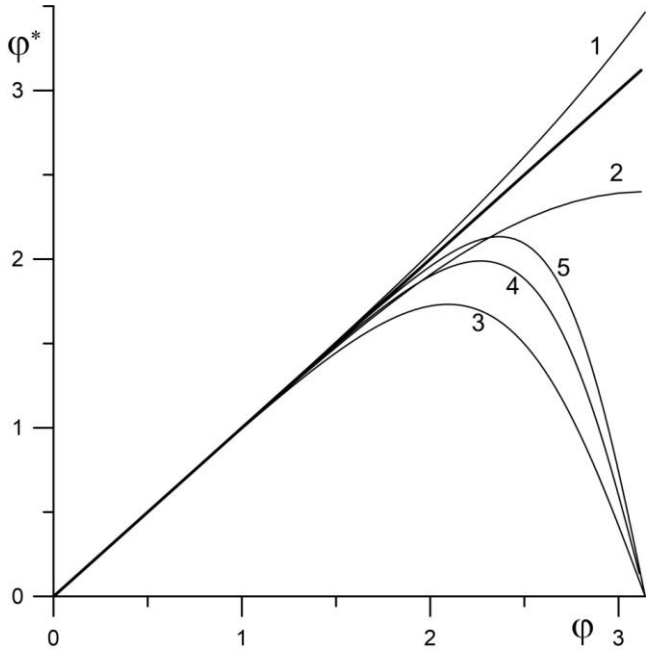

Fig. 2. The dimensionless effective wave number as a function of the dimensionless exact wave number for various symmetric semidiscrete schemes. Curves: 1 - bicompact scheme of the 4th order of accuracy; 2 - compact scheme CCS-T4 of the 4th order of accuracy [4]; 3 - tridiagonal standard compact scheme of the 4th order of accuracy [20]; 4 – tridiagonal standard compact scheme of the 6th order of accuracy [20]; 5 - tridiagonal compact scheme of the 8th order of accuracy [20]. The thick line shows an ideal relationship $\varphi^* = \varphi$.

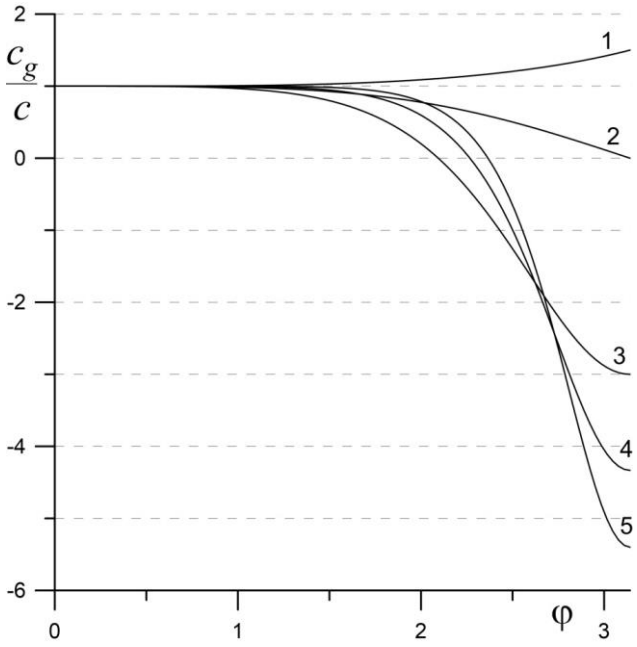

Fig. 3. The dimensionless numerical group velocity as a function of the dimensionless exact wave number for various symmetric semidiscrete schemes. Curves: 1 - bicompact scheme of the 4th order of accuracy; 2 - compact scheme CCS-T4 of the 4th order of accuracy [4]; 3 - tridiagonal standard compact scheme of the 4th order of accuracy [20]; 4 - tridiagonal standard compact scheme of the 6th order of accuracy [20]; 5 - tridiagonal compact scheme of the 8th order of accuracy [20].

For the eighth-order accurate bicompact scheme (30) with the coefficient matrix $\mathbf{A}_8$, Eq. (35) with $R(z) = R_8(z)$ can be transformed into

$$(\varphi^*)^4 + 20\cot(\varphi/2)(\varphi^*)^3 - 180(\varphi^*)^2 - 840\cot(\varphi/2)\varphi^* + 1680 = 0\,. \qquad (41)$$

From Eq. (41), φ can be explicitly expressed in terms of φ^* as

$$\varphi = 2\arctan\left(\frac{20\varphi^*\left[42 - (\varphi^*)^2\right]}{(\varphi^*)^4 - 180(\varphi^*)^2 + 1680}\right). \qquad (42)$$

Dependences (40) and (42) for $\varphi \in [-\pi, \pi]$ are depicted by five curves in Figs. 4 and 5, respectively. These curves do not intersect; moreover, only one of them (curve *1*) passes through the point (0,0) in the (φ, φ^*) plane and corresponds to the physical solution.

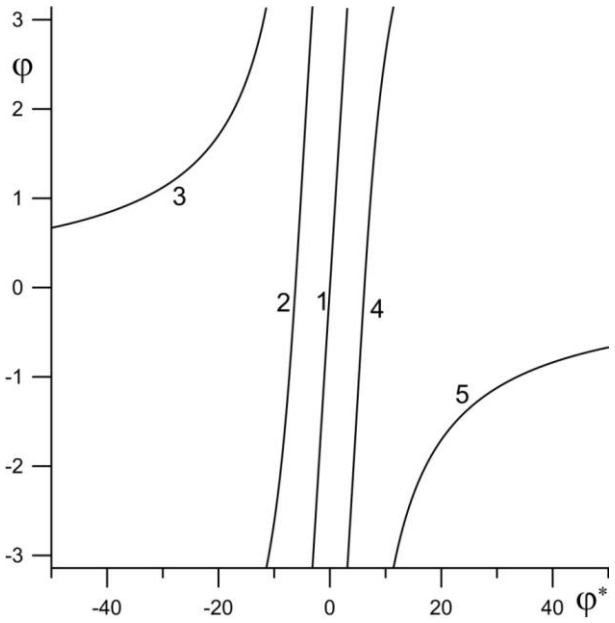

Fig. 4. The dimensionless exact wave number as a function of the dimensionless effective wave number for the semidiscrete bicompact scheme of the 6th order of accuracy.

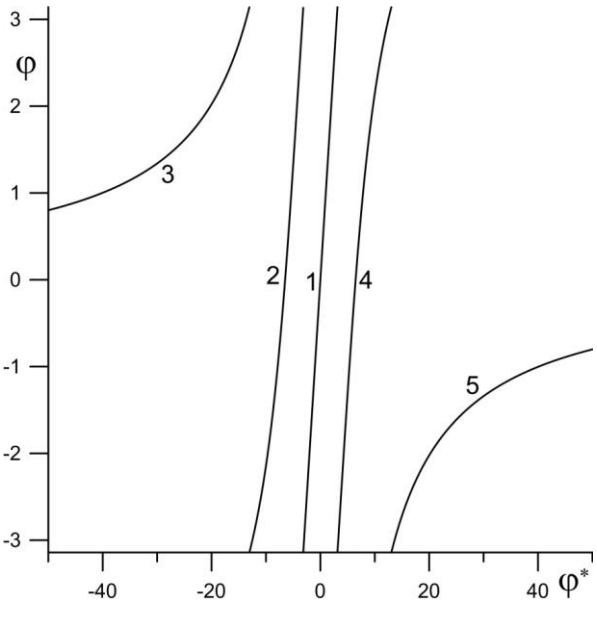

Fig. 5. The dimensionless exact wave number as a function of the dimensionless effective wave number for the semidiscrete bicompact scheme of the 8th order of accuracy.

Figure 6 shows $\left|\varphi^*/\varphi - 1\right|$ as a function of φ for the sixth-order accurate semidiscrete bicompact scheme and the semidiscrete compact scheme CCS-T6 [4] of the same order, which is the best out of the linear schemes for the transport equation found in the literature in the sense that it has a small phase error $\left|\varphi^*/\varphi - 1\right|$ for all $\varphi \in [0, \pi]$. It can be seen that the maximum phase error of the bicompact scheme is

1/16 as large as that of CCS-T6 [4] for $\varphi=\pi$, which corresponds to the shortest wavelength resolvable by the grid. Figure 7 presents the plot of c_g/c against φ for the same schemes as in Fig. 6. Note that, according to the group velocity control theory for shock-capturing schemes [21, 22], the sixth-order accurate bicompact scheme and CCS-T6 [4] are of the slow type.

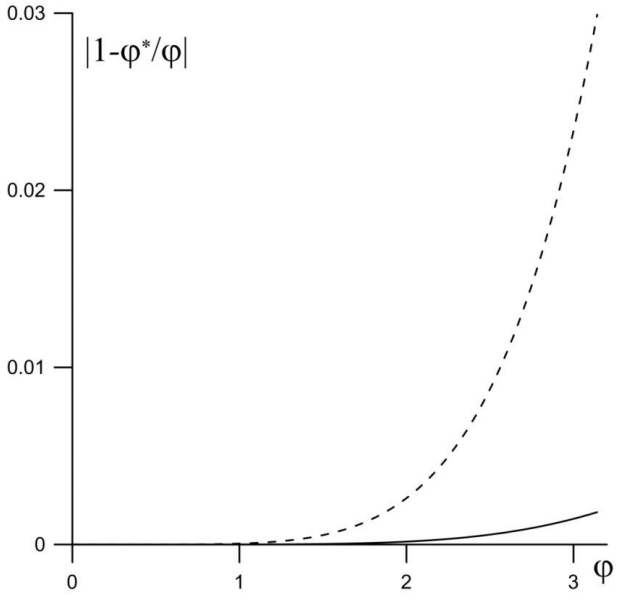

Fig. 6. Phase error of semidiscrete compact schemes. The solid curve shows the dependence of the error on the dimensionless wave number for the bicompact scheme of the 6th order of accuracy, the dashed curve for the compact scheme CCS-T6 of the 6th order of accuracy [4].

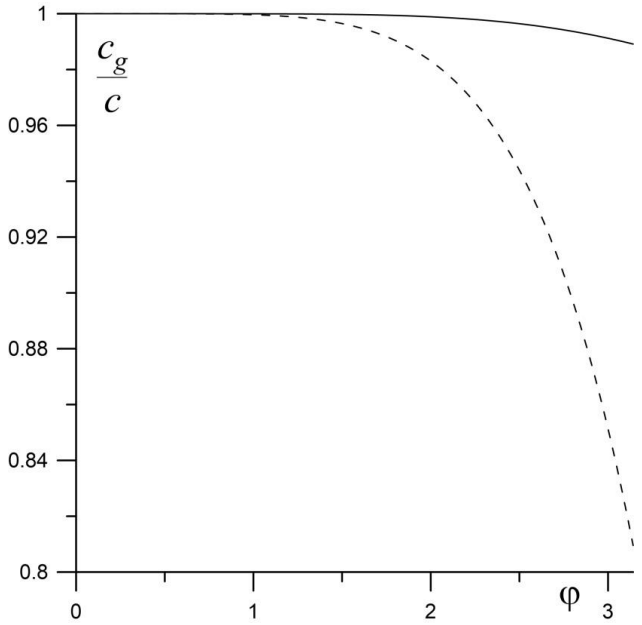

Fig. 7. Dimensionless numerical group velocity of semidiscrete compact schemes. The solid curve shows the dependence of the velocity on the dimensionless wave number for the bicompact scheme of the 6th order of accuracy, the dashed curve for the compact scheme CCS-T6 of the 6th order of accuracy [4].

Figure 8 shows $\left|\varphi^*/\varphi-1\right|$ as a function of φ for the eighth-order accurate semidiscrete bicompact scheme and the semidiscrete compact scheme CCS-T8 [4] of the same order, which is the best out of the linear schemes for the transport equation found in the literature in the sense that it has a small phase error for all $\varphi\in[0,\pi]$. The maximum phase error of the bicompact scheme is 1/27 times as large as that of CCS-T8 [4] for $\varphi=\pi$. Figure 9 presents c_g/c as a function of φ for the same schemes as in Fig. 8. Note that, according to the group velocity control theory for shock capture [21, 22], the eighth-order accurate bicompact scheme is of the fast type, while CCS-T8 [4] is of the slow type.

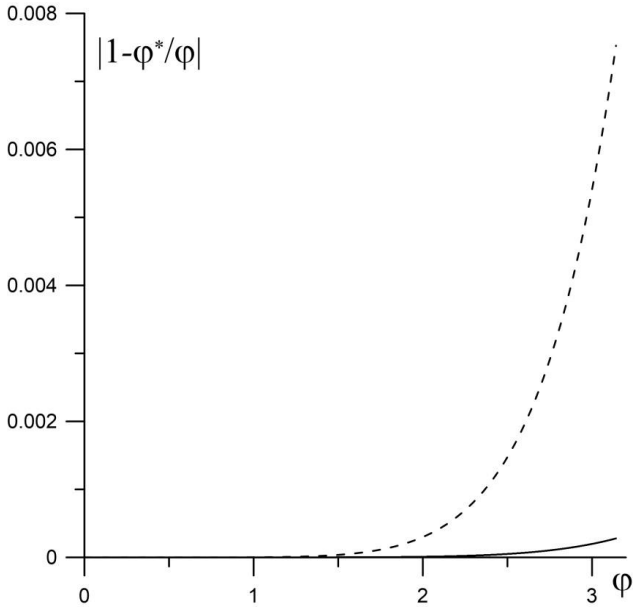

Fig. 8. Phase error of semidiscrete compact schemes. The solid curve shows the dependence of the error on the dimensionless wave number for the bicompact scheme of the 8th order of accuracy, the dashed curve for the compact scheme CCS-T8 of the 8th order of accuracy [4].

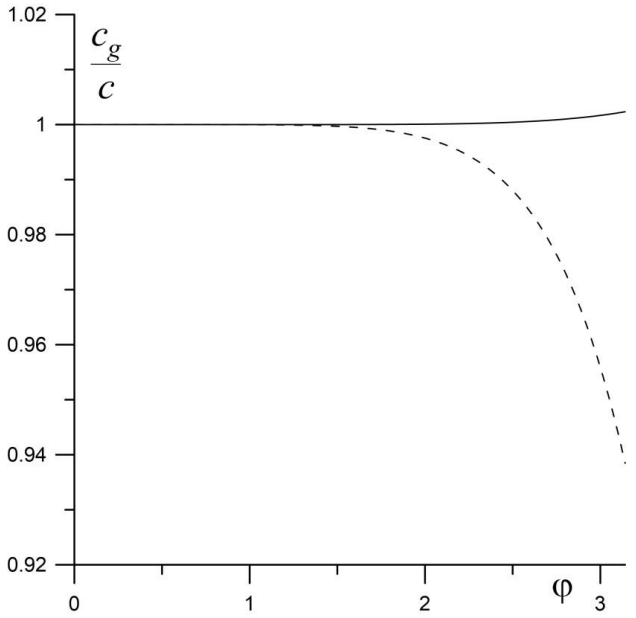

Fig. 9. Dimensionless numerical group velocity of semidiscrete compact schemes. The solid curve shows the dependence of the velocity on the dimensionless wave number for the bicompact scheme of the 8th order of accuracy, the dashed curve for the compact scheme CCS-T8 of the 8th order of accuracy [4].

Note that the dispersion analysis of the semidiscrete bicompact schemes was restricted to a single grid cell, since their stencils are contained within a single cell. As a result, small dispersion error of the bicompact schemes is preserved in the transition from uniform to highly nonuniform grids. In contrast to the bicompact schemes, the stencils of CCS-T4 and CCS-T6 [4] consist of three integer and three half-integer nodes, while the stencil of CCS-T8 [4] is composed of four integer and four half-integer nodes. Thus, the stencils of the schemes from [4] extend over several grid cells, so their spectral properties determined on uniform grids can be approximately transferred only to slightly nonuniform grids [1, 5]. In the case of a highly nonuniform grid, this transfer is not valid.

4. Numerical results

The following test Cauchy problem was used in [23] to evaluate the ability of schemes to correctly reproduce short-wave harmonics on long time intervals when applied to transport equations. The task is to numerically solve the transport equation

$$u_t + u_x = 0 \tag{43}$$

with the initial condition

$$u(x,0)=\left[2+\cos\left(\sigma x\right)\right]\exp\left[-\ln 2\left(\frac{x}{10}\right)^2\right] \tag{44}$$

and the parameter $\sigma = 1.7$ up to the times $t=400$ and $t=800$ on a uniform grid with step $h=1$. For this step size, the parameter σ coincides with φ. It was proposed in [23] that the exact and numerical solutions be compared at $t=400$ and $t=800$.

In this study, problem (43), (44) was solved on the interval $x\in[-50,50]$ with periodic boundary conditions. For time integration, we used the fourth-order accurate singly diagonally implicit RK method with five implicit stages SDIRK54 [24], which is *L*-stable and stiffly accurate. Its Butcher tableau [7] is given by

$$\begin{array}{c|ccccc}
1/4 & 1/4 & & & & \\
0 & -1/4 & 1/4 & & & \\
1/2 & 1/8 & 1/8 & 1/4 & & \\
1 & -3/2 & 3/4 & 3/2 & 1/4 & \\
1 & 0 & 1/6 & 2/3 & -1/12 & 1/4 \\
\hline
 & 0 & 1/6 & 2/3 & -1/12 & 1/4
\end{array}.$$

The application of this method to the system of equations of a semidiscrete bicompact scheme yields an absolutely stable fully discrete difference scheme [7]. The Courant number was specified as CFL = 0.1 for the fourth- and sixth-order bicompact schemes and as CFL = 0.06 for the eighth-order bicompact scheme. It was checked that the time discretization error was much less than the spatial discretization error.

Tables 1-3 present the numerical errors *Err* in the L_1 and L_∞ norms and the local orders of convergence *p* for the numerical solution at *t* = 800 for various *h*. It can be seen that the actual order of convergence is close to the order of accuracy of the scheme in space.

Table 1

Errors and orders of convergence of the fourth-order bicompact scheme for CFL=0.1 **and** $\sigma=1.7$

	Integer nodes				**All nodes**			
h	$\|Err\|_1$	*p*	$\|Err\|_\infty$	*p*	$\|Err\|_1$	*p*	$\|E\|_\infty$	*p*
1	3.58e-1		1.01e+0		3.51e-1		1.01e+0	
1/2	1.61e-1	1.15	9.21e-1	0.14	1.61e-1	1.12	9.33e-1	0.11
1/4	1.09e-2	3.88	6.29e-2	3.87	1.09e-2	3.88	6.34e-2	3.87
1/8	6.88e-4	3.98	4.00e-3	3.97	6.89e-4	3.99	4.00e-3	3.98

Table 2

Errors and orders of convergence of the sixth-order bicompact scheme for CFL=0.1 **and** $\sigma = 1.7$

	Integer nodes				**All nodes**			
h	$\|Err\|_1$	p	$\|Err\|_\infty$	p	$\|Err\|_1$	p	$\|Err\|_\infty$	p
1	1.64e-2		9.59e-2		1.66e-2		9.59e-2	
1/2	2.89e-4	5.83	1.65e-3	5.86	2.91e-4	5.83	1.68e-3	5.83
1/4	4.70e-6	5.94	2.67e-5	5.95	4.71e-6	5.95	2.72e-5	5.95
1/8	7.76e-8	5.92	4.40e-7	5.92	7.74e-8	5.93	4.41e-7	5.95

Table 3

Errors and orders of convergence of the eighth-order bicompact scheme for CFL=0.06 **and** $\sigma = 2.5$

	Integer nodes				**All nodes**			
h	$\|Err\|_1$	p	$\|Err\|_\infty$	p	$\|Err\|_1$	p	$\|Err\|_\infty$	p
1	1.70e-2		9.31e-2		1.71e-2		9.82e-2	
1/2	7.31e-5	7.86	4.05e-4	7.84	7.31e-5	7.87	4.22e-4	7.86
1/4	2.57e-7	8.15	1.42e-6	8.15	2.53e-7	8.17	1.43e-6	8.20

Figure 10 (circles) presents the numerical solution of problem (43), (44) with $\sigma = 1.7$ at the time $t = 800$ as produced by the fourth-order bicompact scheme with two step sizes: (a) $h = 1/2$ and (*b*) $h = 1/4$. The solid curve depicts the exact solution. It can be seen that the exact and numerical solutions differ noticeably at $h = 1/2$. For a smaller step size ($h = 1/4$), the exact and numerical solutions are visually close to each other.

Figures 11 and 12 show the numerical results for problem (43), (44) at $t = 800$ as produced by the sixth- and eighth-order bicompact schemes, respectively, with $h = 1$. The parameter σ was specified as $\sigma = 1.7$ for the sixth-order scheme and as $\sigma = 2.5$ for the eighth-order scheme. The exact solution is depicted by solid curves. It can be seen that the wave packet is transferred over the grid at the correct velocity without distortions and the numerical solution is close to the exact one.

Figure 13 presents the numerical solution of problem (43), (44) at $t = 800$ for $\sigma = 2.5$ as produced by the eighth-order accurate bicompact scheme on a nonuniform spatial grid. The first two mesh sizes were set to 0.5, while the subsequent ones alternated as 1.0, 0.5, 1.0, 0.5, …. Figure 13 shows that the wave packet is transferred over this grid without distortions and the numerical solution is close to the exact one.

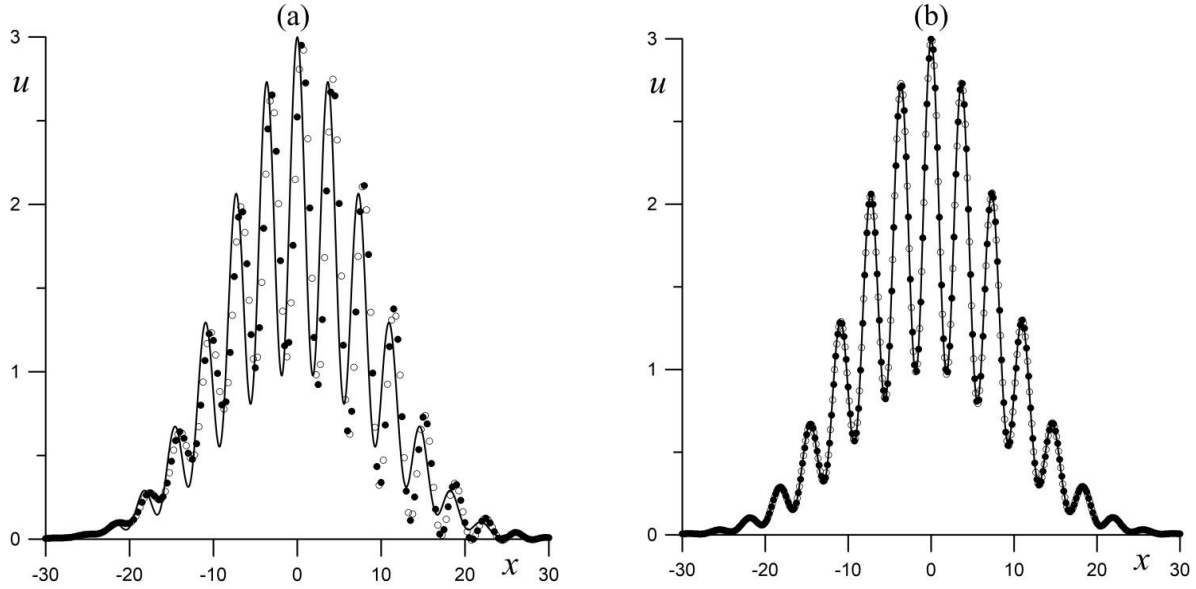

Fig. 10. The solution profiles in the wave packet transfer problem at time t = 800 for $\sigma = 1.7$. The solid line is the exact solution. The numerical solution, calculated using the bicompact scheme of the 4th order, is shown by black circles in integer nodes, and by empty circles in auxiliary nodes. Variants of calculations: (a) h = 1/2, (b) h = 1/4.

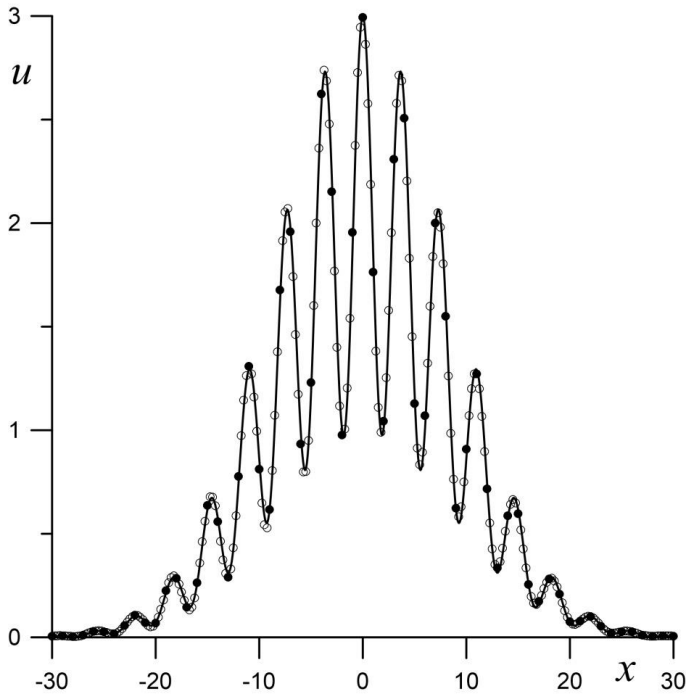

Fig. 11. The solution profiles in the wave packet transfer problem at time t = 800 for $\sigma = 1.7$. The solid line is the exact solution. The numerical solution, calculated using the bicompact scheme of the 6th order on a grid with a step h = 1, is shown by black circles in integer nodes, and by empty circles in auxiliary nodes.

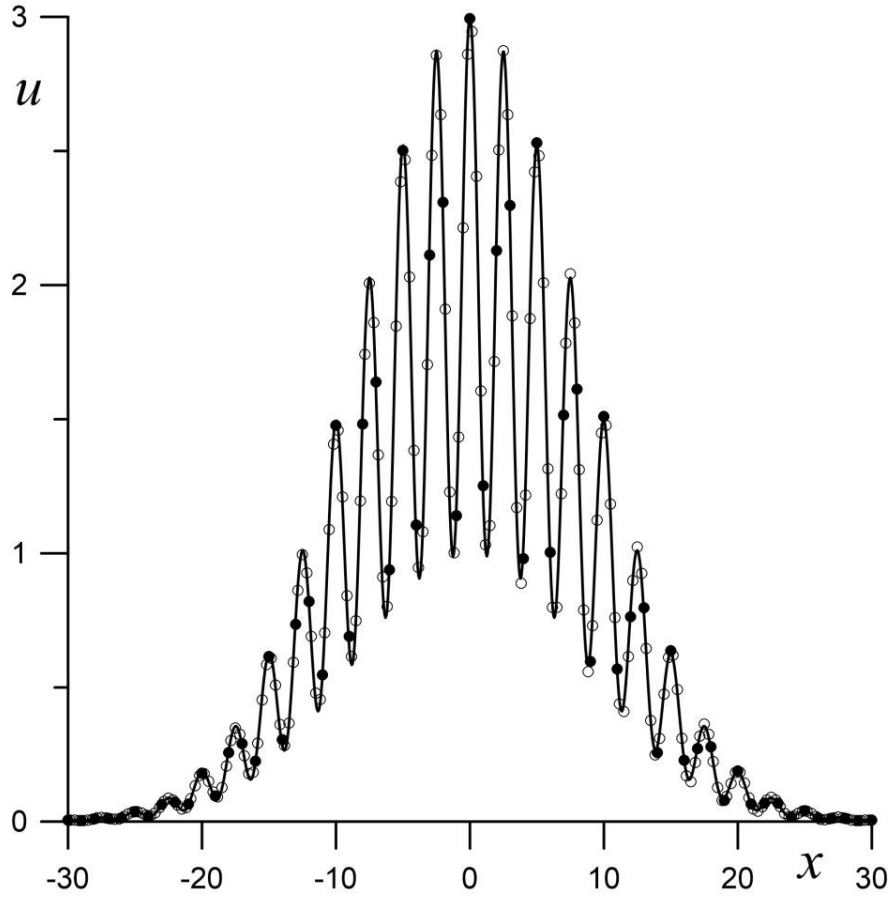

Fig. 12. The solution profiles in the wave packet transfer problem at time t = 800 at $\sigma = 2.5$. The solid line is the exact solution. The numerical solution, calculated using the 8th order bicompact scheme on a grid with step h = 1, is shown by black circles in the integer nodes, and by empty circles in the auxiliary nodes.

Consider two problems similar to the transport of pulse over a nonuniform grid (see [19]).

In the first problem, Eq. (43) was solved on the interval $x \in [0,4]$ with the initial condition

$$u(x,0) = \begin{cases} \left(0.25 - (x-0.5)^2\right)^{11}, & x \in [0,1], \\ 0, & x \notin [0,1]. \end{cases} \tag{45}$$

and periodic boundary conditions. A piecewise uniform grid with $h = 0.05$ on the interval $[0,2]$ and $h = 0.5$ on $[2,4]$ was used in the computations.

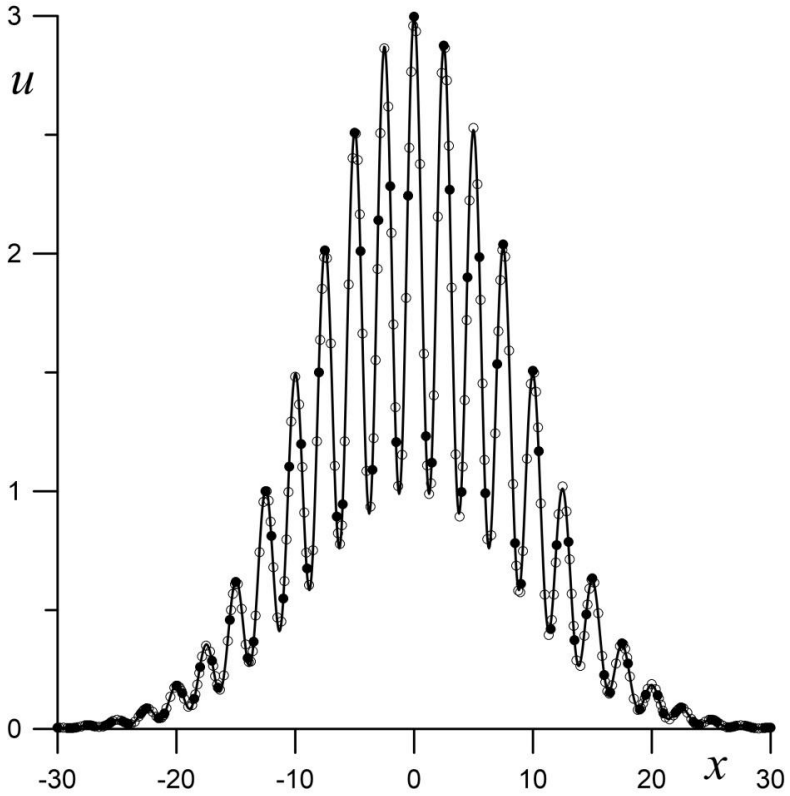

Fig. 13. The solution profiles in the wave packet transfer problem at time t = 800 for $\sigma = 2.5$. The solid line is the exact solution. The numerical solution, calculated using the bicompact scheme of the 8th order on a non-uniform grid with alternating steps h = 1/2 and h = 1, is shown by black circles in the integer nodes, and by empty circles in the auxiliary nodes.

Figure 14 presents the numerical solutions of problem (43), (45) at (a) t = 1 and (b) $t = 2$ as obtained with the eighth-order semidiscrete bicompact scheme. Time integration was based on the fourth-order accurate SDIRK54 method [24] with step $\tau = 0.01$. The plots presented show that the pulse is transferred by the scheme without distortions and no spurious waves are observed near $x = 2$.

The second problem was computed on the same spatial interval $x \in [0,4]$ with the same piecewise uniform grid, but for the system of acoustic equations

$$\mathbf{u}_t + \bar{\mathbf{A}}\mathbf{u}_x = 0,\ \mathbf{u} = \begin{pmatrix} u_1 \\ u_2 \end{pmatrix},\ \bar{\mathbf{A}} = \begin{bmatrix} 0 & 1 \\ 1 & 0 \end{bmatrix} \tag{46}$$

with initial conditions

$$\mathbf{u}(x,0) = \begin{pmatrix} \sin(\pi x)^2 - \cos(\pi x) \\ \sin(\pi x)^2 + \cos(\pi x) \end{pmatrix} \tag{47}$$

and periodic boundary conditions.

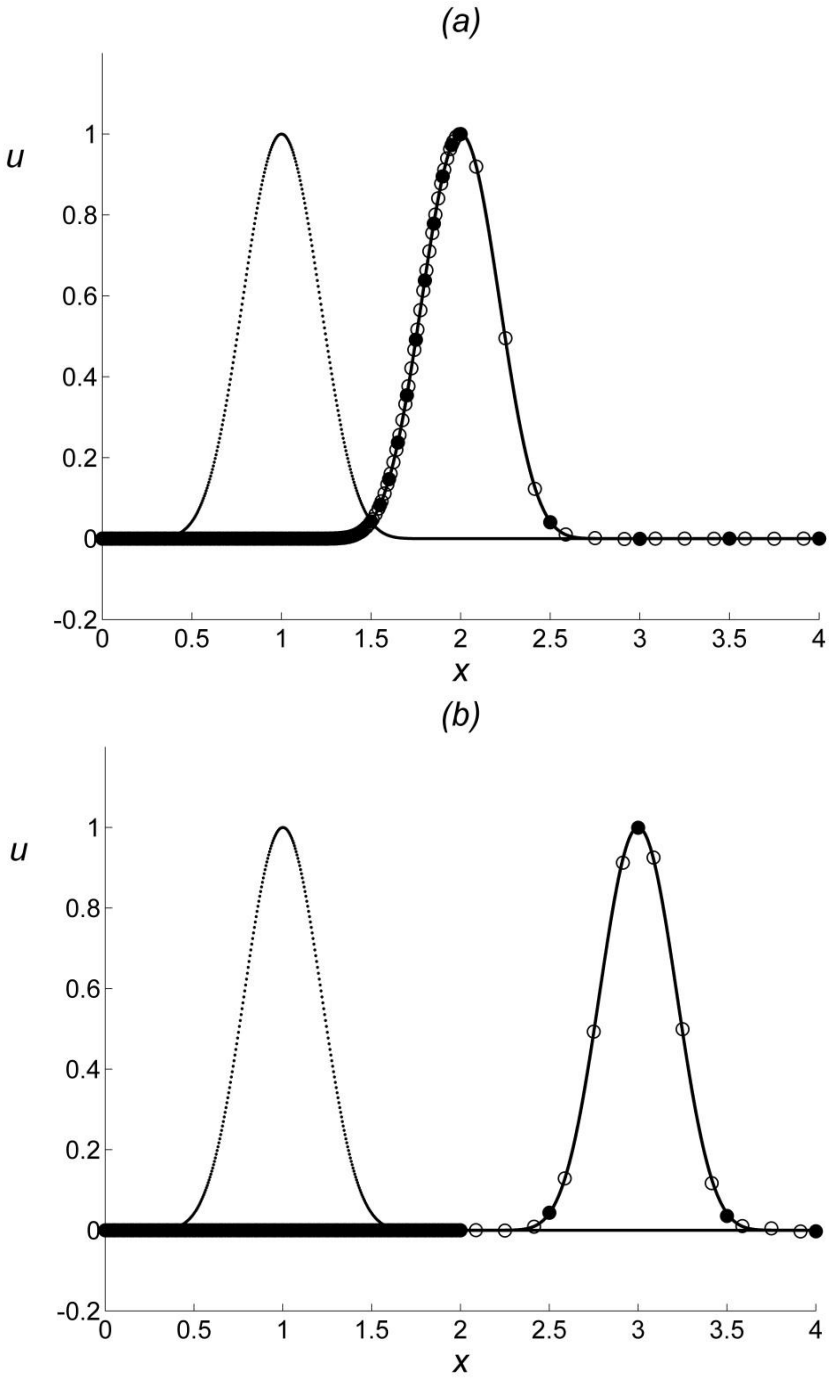

Fig. 14. Profiles of solutions in the problem of impulse transfer over a substantially non-uniform grid. The dotted line is the initial condition, the solid line is the exact solution at (a) $t = 1$, (b) $t = 2$. Markers show a numerical solution at the same time: black circles in integer nodes, and empty circles in auxiliary nodes.

In Figs. 15a and 15b, markers show the numerical results for the second problem as produced by the same bicompact scheme as for the first problem with the same time step. Inspection of Fig. 15 shows that the bicompact scheme on a nonuniform grid reproduces the solution components u_1 and u_2 without distortions.

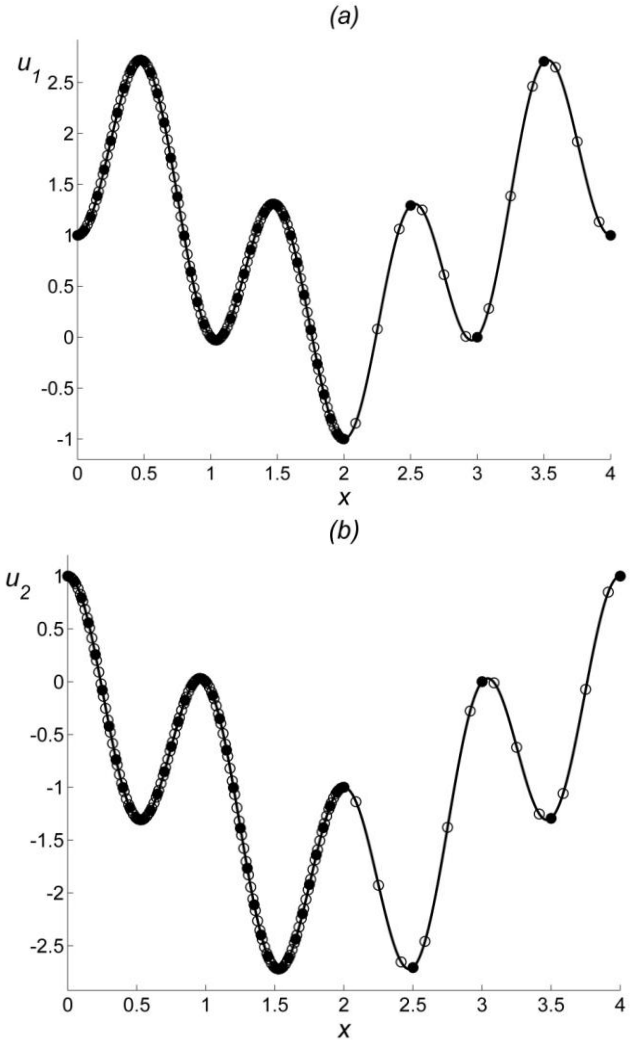

Fig. 15. The solution of the problem (46), (47) at $t = 4$: (a) the first component of the solution, (b) the second component of the solution. Solid lines show the exact solutions. Markers show a numerical solution: black circles in integer nodes, and empty circles in auxiliary nodes.

Let us demonstrate the properties of the sixth- and eighth-order bicompact schemes as applied to the transport of a step function (see Example 1 in [21]). Specifically, the linear transport equation (43) is solved with initial conditions

$$u(x,0)=\begin{cases}1,\ 0\le x<\dfrac{5}{12},\\ 0,\ \dfrac{5}{12}\le x\le 1,\end{cases}$$

on a uniform grid with spatial step $h = 1/200$ up to the time step $N = 500$ for CFL = 0.1. In this work, this problem was solved using the semidiscrete bicompact schemes of sixth and eighth orders of accuracy in space. The time integration of the problem

was based on the well-known three-stage singly diagonally implicit RK scheme SDIRK33, which is third-order accurate in time [25].

Figures 16a and 17a present the basic components of the numerical solution, i.e., the grid functions at integer nodes. It can be seen that they are nearly monotone functions. This behavior of these components agrees with the monotonicity conditions (17) satisfied for the stability function of the spatial integration scheme (7), which was used to construct the bicompact schemes.

Figures 16b and 17b show the oscillations in the numerical solution associated with its auxiliary components determined at fractional nodes. These oscillations have small amplitudes and are localized near the discontinuity of the exact solution, which is depicted by solid lines. The results presented in Figs. 16b and 17b confirm the group velocity control theory for shock-capturing schemes [21, 22]. The sixth-order bicompact scheme with a group velocity lower than the exact one generates oscillations mainly behind the moving discontinuity. The eighth-order bicompact scheme with a group velocity higher than the exact one generates oscillations mainly ahead of the moving discontinuity. A hybrid scheme [26, 27] can be used to eliminate the oscillations from the numerical solution at every time level. However, the bicompact schemes involve an internal filter: the basic component of the numerical solution is nearly monotone. This component can be treated as a filtered solution. An important point to remember in computations based on symmetric bicompact schemes is that numerical dissipation has to be controlled by choosing a suitable time integration procedure.

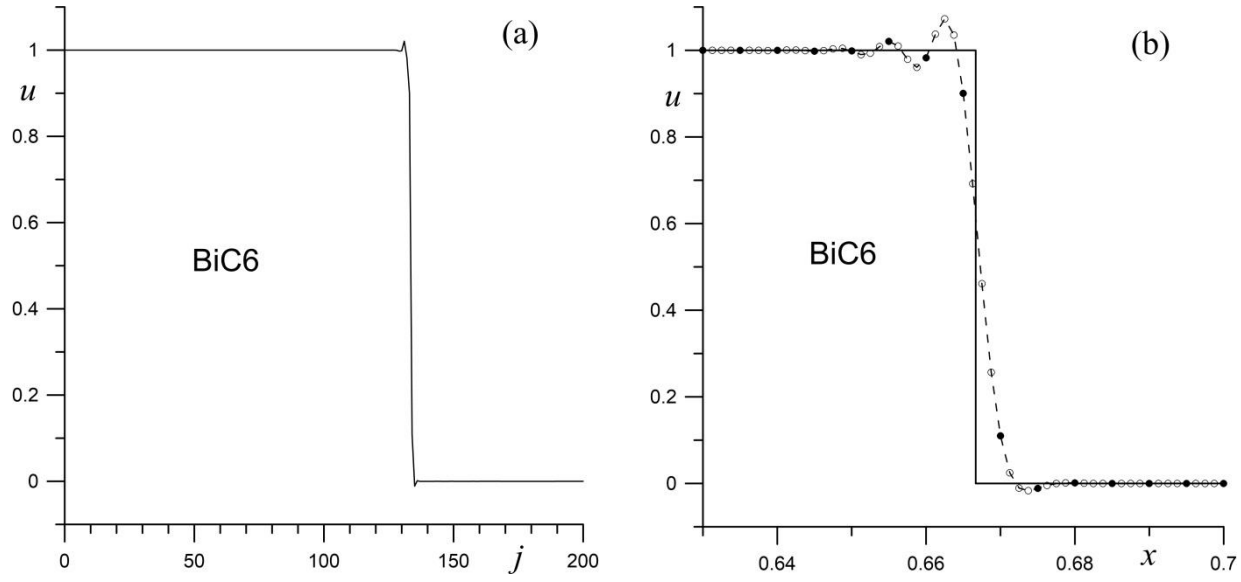

Fig. 16. The solution of the problem of the transfer of the step function, calculated using the bicompact scheme of the sixth order BiC6. (a) Dependence of the numerical solution u in integer nodes on the node number j. (b) Solution u as a function of x near the solution discontinuity: black circles show the values of the numerical solution in integer nodes, empty circles in auxiliary nodes. Solid line is the exact solution.

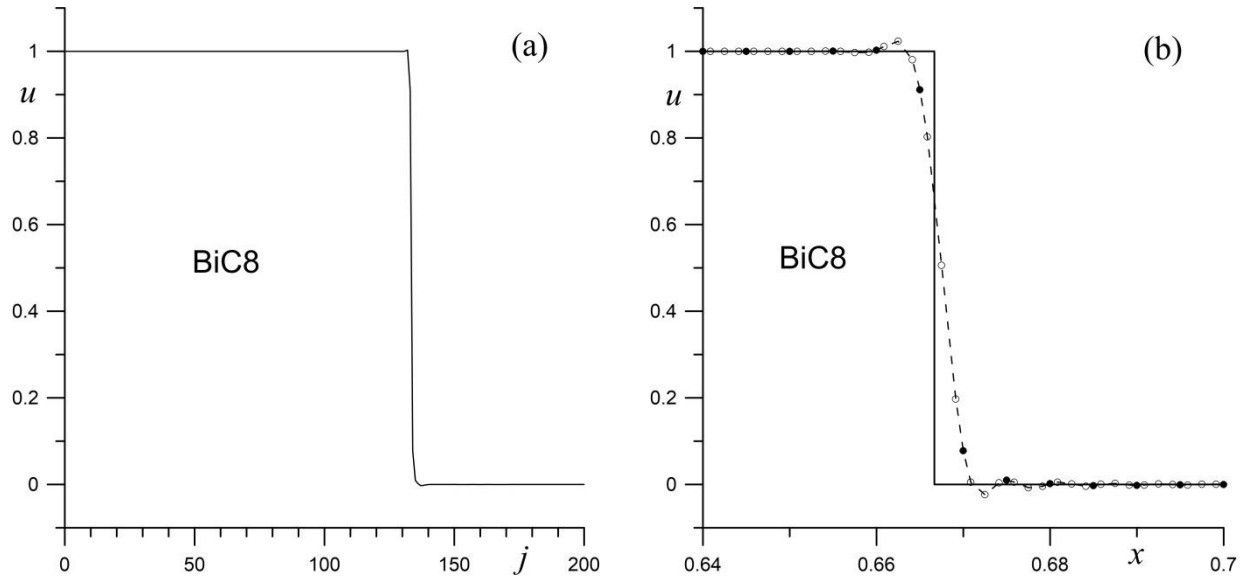

Fig. 17. The solution of the problem of the transfer of the step function, calculated using the bicompact scheme of the eighth order BiC8. (a) Dependence of the numerical solution u in integer nodes on the node number j. (b) Solution u as a function of x near the solution discontinuity: black circles show the values of the numerical solution in integer nodes, empty circles in auxiliary nodes. Solid line is the exact solution.

5. Conclusion

We have presented the dispersion analysis of schemes of fourth to eighth orders of accuracy from the proposed family of semidiscrete symmetric bicompact schemes designed for the numerical solution of the quasilinear transport equation. It was shown that the phase error of the sixth- and eighth-order bicompact schemes does not exceed 0.2% and 0.03%, respectively, in the entire range of dimensionless wave numbers. A comparison of the sixth- and eighth-order semidiscrete bicompact schemes with the compact ones from [4] showed that the maximum phase error of the latter is 16 and 27 times greater than that of the former, respectively. The presented numerical examples demonstrated the ability of the bicompact schemes to adequately simulate short wave propagation on highly nonuniform grids at long times.

Bibliographic list

1. Colonius T., Lele S.K. Computational aeroacoustics: progress on nonlinear problems of sound generation // Prog. Aerosp. Sci. 2004. V. 40. P. 345–416.

2. Ekaterinaris J.A. High-order accurate, low numerical diffusion methods for aerodynamics // Prog. Aerosp. Sci. 2005. V. 41. P. 192–300.

3. Kurbatskii K.A., Mankbadi R.R. Review of computational aeroacoustics algorithms // Int. J. Comput. Fluid Dyn. 2004. V. 18. P. 533-546.

4. Liu X., Zhang S., Zhang H., Shu C.-W. A new class of central compact schemes with spectral-like resolution I: Linear schemes // J. Comput. Phys. 2013. V. 248. P. 235–256.

5. Bogey C., Bailly C. A family of low dispersive and low dissipative explicit schemes for flow and noise computations // J. Comput. Phys. 2004. V. 194. P. 194–214.

6. Rogov B.V., Mikhailovskaya M.N. Monotone high-order accurate compact scheme for quasilinear hyperbolic equations // Dokl. Math. 2011. V. 84. P. 747–752.

7. Hairer E., Wanner G. Solving Ordinary Differential Equations II: Stiff and Differential-Algebraic Problems. Berlin: Springer-Verlag, 1996.

8. Mikhailovskaya M.N., Rogov B.V. Monotone compact running schemes for systems of hyperbolic equations // Comput. Math. Math. Phys. 2012. V. 52, No. 4. P. 578–600.

9. Rogov B.V. High-order accurate monotone compact running scheme for multidimensional hyperbolic equations // Comput. Math. Math. Phys. 2013. V. 53, No. 2. P. 205–214.

10. Chikitkin A.V., Rogov B.V., Utyuzhnikov S.V. High-order accurate monotone compact running scheme for multidimensional hyperbolic equations // Appl. Numer. Math. 2015. V. 93. P. 150–163.

11. Chikitkin A.V., Rogov B.V. A sixth-order bicompact scheme with spectral-like resolution for hyperbolic equations // Dokl. Math. 2017. V. 96, No. 2. P. 480–485.

12. Kalitkin N.N., Koryakin P.V. Numerical methods, Book 2: Methods of mathematical physics. Moscow: The publishing center "Academy", 2013 (in Russian).

13. Bragin M.D., Rogov B.V. Iterative approximate factorization of difference operators of high-order accurate bicompact schemes for multidimensional nonhomogeneous quasilinear hyperbolic systems // Comput. Math. Math. Phys. 2018. V. 58, No. 3. P. 295–306.

14. Rogov B.V., Bragin M.D. On spectral-like resolution properties of fourth-order accurate symmetric bicompact schemes // Dokl. Math. 2017. V. 96, No. 1. P. 339–343.

15. Chikitkin A.V., Rogov B.V. Optimized symmetric bicompact scheme of the sixth order of approximation with low dispersion for hyperbolic equations // Dokl. Math. 2018. V. 97, No. 1. P. 90–94.

16. Zingg D.W. Comparison of high-accuracy finite-difference methods for linear wave propagation // SIAM J. Sci. Comput. 2000. V. 22, No. 2. P. 476–502.

17. Vichnevetsky R. Wave propagation analysis of difference schemes for hyperbolic equations: a review // Int. J. Numer. Meth. Fluids. 1987. V. 7. P. 409-452.

18. Vichnevetsky R. Wave propagation and reflection in irregular grids for hyperbolic equations // Appl. Numer. Math. 1987. V. 3. P. 133-166.

19. Visbal M.R., Gaitonde D.V. Very high-order spatially implicit schemes for computational acoustics on curvilinear meshes // J. Comput. Acoust. 2001. V. 9. P. 1259-1286.

20. Lele S.K. Compact Finite Difference Schemes with Spectral-like Resolution // J. Comput. Phys. 1992. V. 103. P. 16-42.

21. Fu D., Ma Y. A high order accurate difference scheme for complex flow // J. Comput. Phys. 1997. V. 134. P. 1–15.

22. Li X., Fu D., Ma Y. Optimized group velocity control scheme and DNS of decaying compressible turbulence of relative high turbulent Mach number // Int. J. Numer. Meth. Fluids. 2005. V. 48. P. 835–852.

23. Tam C.K.W. Benchmark problems – category 1. Problem 1–aliasing // In: NASA/CP-2004-212954. 2004. P. 3.

24. Skvortsov L.M. Diagonally implicit Runge–Kutta FSAL methods for stiff and differential-algebraic systems // Matem. Mod. 2002. V. 14, No. 2. P. 3–17 (in Russian).

25. Alexander R. Diagonally implicit Runge-Kutta methods for stiff O.D.E.'s // SIAM J. Numer. Anal. 1977. V. 14. P. 1006–1021.

26. Bragin M.D., Rogov B.V. Minimal dissipation hybrid bicompact schemes for hyperbolic equations // Comput. Math. Math. Phys. 2016. V. 56, No. 6. P. 947–961.

27. Bragin M.D., Rogov B.V. A new hybrid scheme for computing discontinuous solutions of hyperbolic equations // Keldysh Institute Preprints. 2016. No. 22. 20 p. URL: http://library.keldysh.ru/preprint.asp?id=2016-22&lg=e.